Phonon-Bottleneck Enhanced Exciton Emission in 2D Perovskites

ADVANCED ENERGY MATERIALS
www.advenergymat.de

Phonon-Bottleneck Enhanced Exciton Emission in 2D Perovskites

Joshua J. P. Thompson, Mateusz Dyksik, Paulina Peksa, Katarzyna Posmyk, Ambjörn Joki, Raul Perea-Causin, Paul Erhart, Michał Baranowski, Maria Antonietta Loi, Paulina Plochocka, and Ermin Malic**

Layered halide perovskites exhibit remarkable optoelectronic properties and technological promise, driven by strongly bound excitons. The interplay of spin-orbit and exchange coupling creates a rich excitonic landscape, determining their optical signatures and exciton dynamics. Despite the dark excitonic ground state, surprisingly efficient emission from higher-energy bright states has puzzled the scientific community, sparking debates on relaxation mechanisms. Combining low-temperature magneto-optical measurements with sophisticated many-particle theory, the origin of the bright exciton emission in perovskites is elucidated by tracking the thermalization of dark and bright excitons under a magnetic field. The unexpectedly high emission is clearly attributed to a pronounced phonon-bottleneck effect, considerably slowing down the relaxation toward the energetically lowest dark states. It is demonstrated that this bottleneck can be tuned by manipulating the bright-dark energy splitting and optical phonon energies, offering valuable insights and strategies for controlling exciton emission in layered perovskite materials that is crucial for optoelectronics applications.

1. Introduction

Hybrid metal-halide perovskites represent a unique material system,[1,2] bridging the electronic properties of epitaxial and organic semiconductors. They emerged as revolutionary materials for photovoltaics,[3] before a plethora of other possible applications were proposed, from light emission[4] to quantum optical technologies,[5,6] where perovskite nanostructures show particular promise.[7–9] Both nanocrystals and two-dimensional (2D) layered perovskites are known for their superior emissive properties.[9–11] Their quantum emission efficiency is one or two orders of magnitude higher than in epitaxial inorganic semiconductors, however the origin of this technologically important characteristic is still the subject of ongoing research and debate.[10–12]

The optical response of perovskites is governed by excitons exhibiting a characteristic fine structure comprising bright triplet and dark singlet states.[10,11,13,14] Recent studies have shown that the dark state is situated several to tens of meV below the bright states.[5,10,15,16] Despite this significant splitting, perovskites exhibit surprisingly intense photoluminescence (PL) emission even at cryogenic temperatures[9–11,17] making them very attractive for quantum technology. Moreover, in nanocrystals, intense emission is simultaneously observed for all bright states even though they are also separated by several meV.[10,14] This emissive behavior indicates that the exciton population in perovskites does not follow Boltzmann statistics, however, the origin of this high bright-state occupation has remained elusive. Thus, an in-depth

J. J. P. Thompson, E. Malic
Department of Physics
Philipps-Universität Marburg
Renthof 7, 35032 Marburg, Germany
E-mail: ermin.malic@uni-marburg.de

J. J. P. Thompson
Department of Materials Science and Metallurgy
University of Cambridge
Cambridge CB3 0FS, UK

The ORCID identification number(s) for the author(s) of this article can be found under https://doi.org/10.1002/aenm.202304343

DOI: 10.1002/aenm.202304343

M. Dyksik, P. Peksa, K. Posmyk, M. Baranowski, P. Plochocka
Department of Experimental Physics
Faculty of Fundamental Problems of Technology
Wroclaw University of Science and Technology
Wroclaw 50-370, Poland
E-mail: paulina.plochocka@lncmi.cnrs.fr

P. Peksa, K. Posmyk, P. Plochocka
Laboratoire National des Champs Magnétiques Intenses, EMFL, CNRS UPR 3228, Université Grenoble Alpes, Université Toulouse, Université Toulouse 3, INSA-T
Grenoble 38042 , Toulouse 31400 France

A. Joki, R. Perea-Causin, P. Erhart
Department of Physics
Chalmers University of Technology
Gothenburg 412 96, Sweden

M. A. Loi
Zernike Institute for Advanced Materials
University of Groningen
Nijenborgh 4, Groningen 9747 AG, The Netherlands

quantum mechanical modeling of exciton relaxation dynamics including the interplay of the exciton fine structure and scattering with phonons is required to fully exploit and design perovskites for light emission applications.

Here, we address this problem for an archetypical perovskite, $(PEA)_2PbI_4$, where PEA stands for phenylethylammonium. This 2D layered perovskite demonstrates significant splitting between the bright and dark states (≈20meV)[15,16] which is off-resonant with optical phonon modes,[18–22] indicating a possible bottleneck effect. Using a microscopic and material-specific many-particle theory, we explore the formation, relaxation and decay dynamics of excitons in this structure and show that the energy mismatch between the fine structure of exciton and phonons leads to a pronounced phonon-bottleneck effect. The consequence is an inefficient exciton relaxation to the energetically lowest dark state resulting in an enhanced non-thermal population of bright excitons, explaining the surprisingly high cryogenic PL emission. We find an excellent agreement between theoretical predictions and temperature-dependent magneto-optical spectroscopy measurements offering access to the dark exciton population. Our work provides a comprehensive microscopic picture of the phonon-bottleneck effect between bright and dark exciton states in the family of 2D perovskites, explaining why these materials exhibit strong emission at low temperatures despite their dark ground state.

2. Results

2.1. Exciton Energy Landscape

Strong spin-orbit coupling and exchange interaction in perovskite nanocrystals and 2D perovskites give rise to an exciton fine-structure comprised of a dark singlet and bright triplet states.[11,13,14,23–25] Recent experimental studies have provided extensive characterization of exciton states, as well as their energy spacing in $(PEA)_2PbI_4$.[15,16,26,27] In layered perovskites (see **Figure 1**a) the lowest energy dark state X_D is typically separated by $\approx 15-20$ meV from the two in-plane bright states X_+ and X_- and by another ≈1 meV from the out-of-plane polarized grey state X_Z. A schematic of the exciton state structure is presented in Figure 1b. We discuss the impact of different crystal phases in the Supporting Information.

We model the electron-hole interaction with the generalised Keldysh potential[28] (all parameters can be found in Supporting Information). The energy landscape including the material-specific splitting has been determined microscopically by solving the Wannier equation[29,30] before including the impact of the short- and long-range exchange interaction. Our model accurately recovers qualitatively and quantitatively all characteristic features of the exciton fine structure[15,16,25,26,31] observed in the exemplary $(PEA)_2PbI_4$, a reliable basis for studying the excitonic relaxation dynamics.

A quantitative picture of the theoretically predicted (lines) and measured (dots) excitonic landscape can be seen in **Figure 2**a, which shows the spectral shift of the dark, bright and grey states as a function of the applied in-plane magnetic field (Voigt configuration). At zero field, we find a bright-dark splitting, Δ_{BD}, of 21 meV. The magnetic field lifts the degeneracy of the bright in-plane states $X_{+/-}$ and changes their polarization from circularly

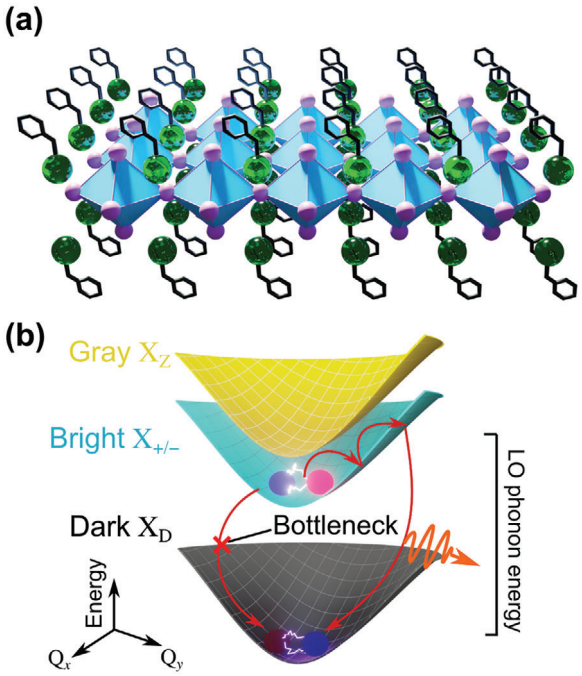

Figure 1. a) Crystal structure of the 2D perovskite $(PEA)_2$ PbI_4. b) Schematic of the exciton fine structure including bright (X_+, X_-), gray (X_Z) and dark exciton states (X_D) and their relaxation dynamics. In particular, the phonon-bottleneck is shown to hinder the scattering between bright and dark excitons.

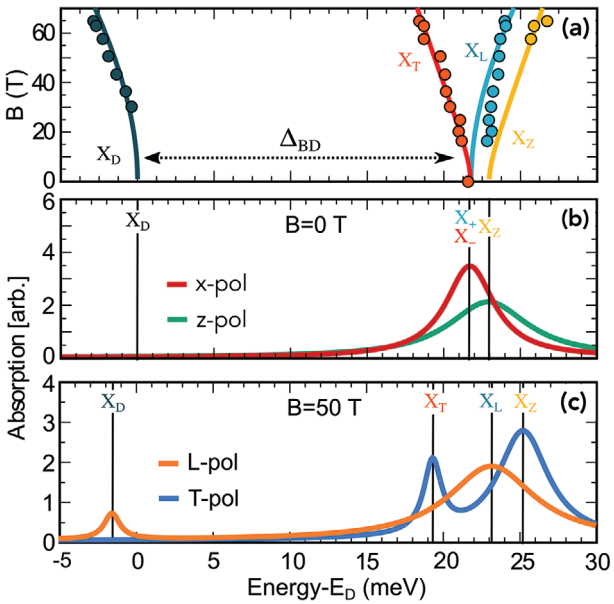

Figure 2. a) Exciton fine-structure of the 2D perovskite $(PEA)_2$ PbI_4 as a function of in-plane magnetic field, calculated (lines) and measured (dots). The bright-dark splitting, Δ_{BD}, is shown with the arrow. As the magnetic field increases, the polarization of longitudinal (X_L) and dark (X_D), as well as the polarization of gray (X_Z) and transverse polarized (X_T) excitons mix. b,c) Absorption spectra at 30 K for $B = 0$ T and $B = 50$ T, respectively. The positions of exciton states are marked with thin vertical lines. Note that without a magnetic field, there are ciruclary polarized states ($X_\pm$) that become linearly polarized ($X_{L,T}$) due to mixing at $B \neq 0$.

to linearly polarized. The new in-plane states are now polarized parallel (longitudinal X_L) and perpendicular (transverse X_T) to the magnetic field. We perform magnetic field and polarization-dependent transmission measurements to experimentally determine the excitonic energy landscape. We find an excellent theory-experiment agreement for the magnetic field dependence of the exciton energy, see Figure 2 a.

The magnetic field mixes the dark X_D and the gray X_Z states with the superposition of the two bright in-plane states,[32] resulting in a partial transfer of the oscillator strength from X_L and X_T to X_D and X_Z states, respectively. To investigate this, we determine the optical absorption spectra (at 30 K) of $(PEA)_2PbI_4$ by numerically evaluating the Elliot formula and second-order Born-Markov equation[28,29,33] (see Supporting Information for more details). In the absence of a magnetic field (B = 0 T), only absorption related to the bright triplet states can be observed: two degenerate circularly polarized states or a grey state, see Figure 2b. For x-polarized absorption (red line in Figure 2b), signatures from the $X_{+/-}$ excitons are observed, while the gray exciton cannot be seen. On the other hand, for z-polarized light (green line) the gray state is visible, while the bright states are not. The enhanced broadening of the z-polarized emission comes from additional phonon scattering channels to the lower-lying bright excitons (see Figure 1b). The lowest energy spin-dark exciton X_D has a vanishing oscillator strength and cannot be seen, however it can be optically accessed in a magnetic field, see Figure 2c. Here, the dark state becomes visible and L- and T-polarized bright excitons are now clearly distinct. Due to its efficient mixing with the X_L state, the dark exciton can be only observed in the L-polarized absorption (orange line), whereas the gray exciton is only visible for T-polarized excitation (blue line) reflecting its mixing with the X_T state.

2.2. Phonon-Bottleneck Effect

Following optical excitation of the bright states, excitons thermalize via scattering within or between excitonic bands. Considering a clean sample in the low-excitation regime, exciton relaxation is driven by phonon-induced scattering. For most semiconductors, fast phonon-mediated scattering leads to a thermalized Boltzmann distribution.[33,34] However, in systems where phonon-assisted scattering is prohibited due to inherent differences between the initial and final states (mismatch of angular momentum, energy or momentum), a non-thermal distribution can arise. In 2D perovskites, strong spin-orbit coupling in the conduction band mixes different states, facilitating scattering between excitons with opposite spin. Another possible origin for a non-thermal distribution is a mismatch between the energy of the initial and final states and the involved phonon energies. In the case of $(PEA)_2PbI_4$, it was observed that the excitonic transition is predominantly coupled to the optical phonon with the energy of ≈35 meV[18,19,22,29,35] that is significantly larger than the bright-dark splitting Δ_{BD} ≈20 meV (c.f. Figure 2a).

As a consequence, to scatter from the bright to the dark states, hot excitons need to be formed with considerable excess energy of at least 15 meV to compensate the energy difference between the bright-dark energy splitting Δ_{BD} and the phonon energy E_{LO}. Therefore, optically excited excitons in the light-cone first need to scatter up to higher-momenta states by absorption of acoustic phonons, see Figure 1b. This process is highly unlikely at cryogenic temperatures resulting in a phonon-bottleneck effect, i.e., exciton cannot scatter to the energetically lowest states and thus cannot build a thermal Boltzmann distribution. Note that while Figure 1b shows a typical initial exciton occupation centred at small momenta, the final exciton distribution is independent of the initial excitation conditions, as excitons get trapped when they reach the minimum of the bright exciton band.

To corroborate this explanation, we derive a coupled set of semiconductor Bloch equations describing the temporal evolution of the momentum-resolved exciton occupation $\hat{N}_n^{\mathbf{Q}}(t)$ based on the Heisenberg equation of motion[33] (see Experimental Section and Supporting Information for details). Here, n and $\mathbf{Q}$ denote the exciton state and its centre-of-mass momentum, respectively. This allows us to track the phonon-mediated relaxation cascade within the excitonic fine structure resolved in time and momentum. We include both acoustic and optical phonons[29] to capture the relaxation dynamics. In the simulations presented here, we have assumed a pulsed excitation (initial population at time $t = 0$). In the SI, we also show calculations for a continously driven system and observe only small quantitative changes in the calculated exciton temperature.

A thermal equilibrium is obtained when the population of excitonic states becomes time-independent. To quantify the final distribution of excitons across the exchange-split states in 2D perovskites, we define an effective excitonic temperature, T_{exc}, as obtained by rearranging the Boltzmann distribution $T_{exc} = \frac{\Delta_{BD}}{k_B}\left[\ln\left(\frac{N_D}{N_+}\right)\right]^{-1}$. The excitonic temperature is determined by the ratio of N_D and N_+ corresponding to the exciton density of the dark and the bright exciton X_D and X_+, respectively. Note that N_+ and N_- are degenerate and thus equally populated at thermal equilibrium without a magnetic field.

By definition, in the case of a Boltzmann distribution, the exciton temperature is equal to the lattice temperature (black line in **Figure 3a**). If excitons are trapped in the higher-energy state, X_+, then the effective exciton temperature will be larger than the lattice temperature reflecting the excess energy of hot excitons. To determine the excitonic temperature, we assume an initial excitation of the X_+ bright state achieved by applying a circularly polarized laser pulse. We then calculate the time- and momentum-resolved population dynamics of the four excitonic states by evaluating the semiconductor Bloch equations until the system is thermalized. In Figure 3a, the effective steady-state temperature of the bright exciton in the $(PEA)_2PbI_4$ is shown as a function of the lattice temperature T. For $T > 110$K, we find that the effective exciton temperature T_{exc} (orange line) coincides with the lattice temperature as determined by the Boltzmann distribution (black line). At lower temperatures, however, we show that T_{exc} clearly deviates from the lattice temperature, approaching a constant value of around 75 K even as $T \to 0K$. This signature is a clear indication of a phonon-bottleneck effect, as excitons cannot relax to the energetically lower state and thus exhibit an excess energy that makes them hotter than the lattice temperature. At higher temperatures, this bottleneck effect can be circumvented by the absorption of acoustic phonons lifting bright excitons to higher states and allowing them to scatter down to the dark state, see Figure 1b.

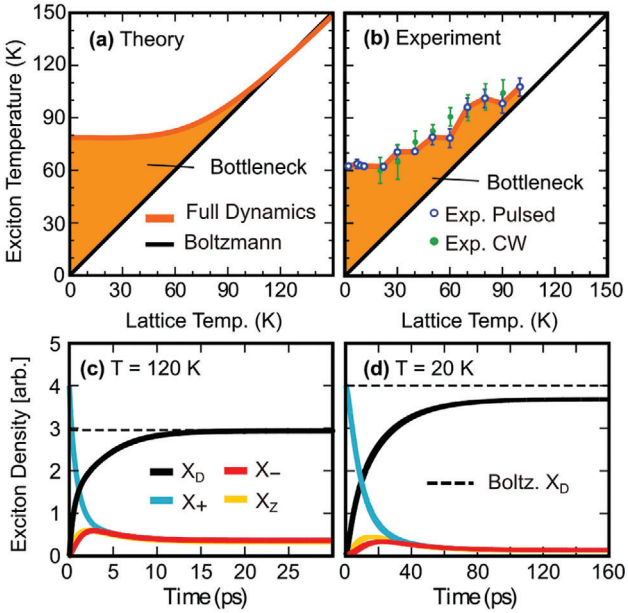

Figure 3. a) Effective steady-state temperature T_{exc} of the bright exciton as a function of the lattice temperature T. The shaded region indicates the phonon-bottleneck effect, i.e., T_{exc} higher than expected from a Boltzman distribution (black line). b) Experimentally obtained exciton temperatures for a pulsed (blue dots) and CW (green dots) excitation. c,d) Theoretical calculations of the temporal evolution of the exciton density at 120 and 20 K, respectively, following a resonant excitation of the bright exciton without a magnetic field. Dashed horizontal line in (c) and (d) shows the expected population of dark exciton assuming a Boltzmann distribution.

We directly compare our theoretical prediction to the experimentally obtained effective exciton temperature in Figure 3b. The latter is obtained by a detailed analysis of the PL response in presence of a magnetic field where dark exciton emission can be directly observed (see Supporting Information for details). The experimental results for pulsed and continuous wave (CW) excitation regime (blue and green points respectively), show a clear deviation from the expected thermal Boltzmann distribution for temperatures lower than 100 K - in excellent agreement with the presented calculation. As the lattice temperature approaches 90 K, we observe that the phonon-bottleneck effect vanishes and the effective exciton temperature goes toward the lattice temperature. This clearly supports the message of a thermally activated phonon-assisted relaxation circumventing the phonon-bottleneck at higher temperatures. Our experimental results show that the phonon-bottleneck is largely independent of the excitation scheme. We compare theoretical calculations of the CW and pulsed excitation regime in the Supporting Information and find a pronounced bottleneck in both cases.

To provide a better understanding of the origin of the phonon-bottleneck, we resolve the simulated population dynamics of different exciton species in Figure 3c,d at 120 and 20 K, respectively. The initial population of the optically excited X_+ exciton (blue line) begins to decay populating the dark (X_D) and gray (X_Z) states. We assume a weak excitation, such that the contribution of exciton–exciton scattering processes is small and can be neglected. There is no direct coupling between the bright states, as this transition would require the conduction and valence band spin to flip simultaneously,[11] which is prohibited due to the absence of spin-orbit coupling in the valence band.[11,36] Instead, excitons from the X_+ state scatter first into the dark or the grey state, before the X_- state can be populated. This explains the delayed onset of the X_- population. Since the bright and grey state are almost energetically equivalent, their final populations are very similar. The dark state is much lower in energy and therefore is the most populated at any temperature. At $T = 120$ K, (Figure 3c), the relative steady-state population follows Boltzmann statistics, as seen from the intersection between the dashed Boltzmann line and the dark exciton population after the equilibrium has been reached. In Figure 3d., the 15 meV required to enable interband scattering between bright and dark states cannot easily be satisfied at 20 K, where the thermal energy $k_BT \approx 6.5$ meV is too low. Therefore, the relaxation process slows down significantly and the quasi-thermal equilibrium is only reached after tens of ps. Note that exciton lifetimes in layered perovskites (≈40 ps[37]) are longer than the typical thermalization time even at 20 K. At such a low temperature, the entire excitonic population would effectively reside within the dark exciton band under Boltzmann statistics, as indicated by the dashed line in Figure 3d. However, in our dynamics simulations, we find the dark exciton population to be significantly lower and hence the population of optically active excitonic states is orders of magnitude larger than expected from a Boltzmann distribution.

To further strengthen the proposed picture of the pronounced phonon-bottleneck effect in $(PEA)_2PbI_4$, we show the experimental PL spectrum as a function of a magnetic field at 20 K - in direct comparison to our theoretical prediction after a stationary distribution has been reached. The magnetic field shifts the excitonic energy levels, but the quantitative effect is relatively small (≈1–2 meV), and hence has little effect on the relaxation. Therefore, we do not observe a significant effect of the magnetic field on the phonon-bottleneck. We distinguish in theory two cases: taking into account the full exciton dynamics (**Figure 4**b) and assuming a Boltzmann distribution (Figure 4c). We fix the bright-dark splitting to about 9 meV as extracted from the PL spectra. The reduced splitting compared to the value found in the absorption spectra[15] (Figure 2c) is likely to be due to disorder, which is characteristic for perovskites[38,39] and polaronic effects.[16,40] The presence of disorder gives rise to a red-shift of the bright exciton and can lead to a crystal distortion changing the crystal bond lengths and altering the exchange coupling that is responsible for the bright-dark energy splitting. Importantly the observed discrepancy in this splitting does not contradict our theoretical predictions and experimental observations of the non-Boltzmann distribution of excitons. As long as the effective phonon energy is larger than the bright-dark exciton splitting, our theory predicts an enhanced temperature of the exciton population, cf. **Figure 5**. Our magneto-optical investigations also clearly point to a non-Boltzman distribution despite the reduced bright-dark splitting in PL.

In the experiment, we observe a transition of the dominant PL signal from the bright to the dark state at about $B = 15$ T. Note that a non-zero oscillator strength of the dark state is observed in the experimental PL at $B = 0$ T (Figure 4a; Figure S3, Supporting Information), which is attributed to crystal distortion and higher-order optical processes.[13,15,25,42] As such the dark state is always slightly visible in experiments. Therefore, we add a non-zero optical matrix element for the dark state also in our simulations.

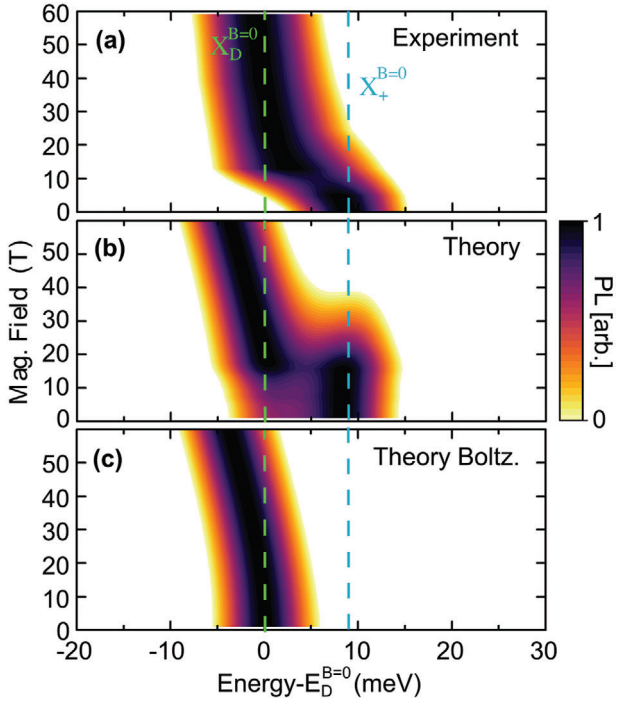

Figure 4. a) Normalized experimental PL spectra as a function of magnetic field at T= 40 K. Theoretically predicted steady-state PL considering the full exciton dynamics (b) and assuming a Boltzmann distribution (c). Dominant exciton resonances at zero magnetic field are indicated with dashed vertical lines.

As the magnetic field is increased, the mixing between the bright and dark states becomes more efficient, such that previously dark exciton gains a progressively larger bright exciton component even dominating the PL spectrum above a certain critical value of the magnetic field. In theory, this occurs at larger values considering the full dynamics (Figure 4b), whereas the dark state dominates already at zero field when assuming a Boltzmann distribution (Figure 4c). This is caused by the much larger

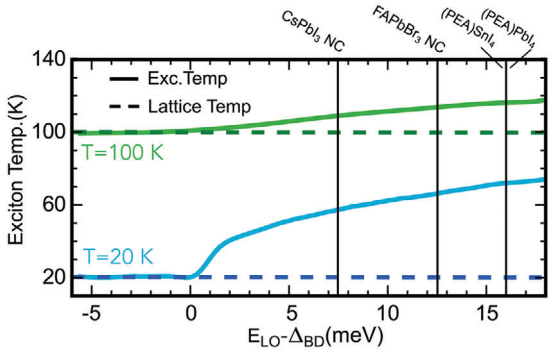

Figure 5. Demonstration of a raised effective exciton temperature as a function of the offset between the optical phonon energy (E_{LO}) and the dark-bright energy splitting (Δ_{BD}). For a vanishing offset, the exciton temperature matches the lattice temperature (dashed line). Examples of offsets measured in other materials are marked with vertical lines including $CsPbI_3$ nanocrystal (NC),[5,41] $FAPbBr_3$ NC,[10] $(PEA)SnI_4$,[15] and $(PEA)PbI_4$ (this work).

population of the energetically lowest dark exciton provided that there is no phonon-bottleneck. The situation is different when considering the full dynamics, where excitons are trapped in the bright state and cannot scatter further down to the dark exciton, see Figure 3. The interplay between the relative population of bright and dark excitons and the brightening of the dark exciton in the presence of a magnetic field determines which exciton dominates the PL. The theoretical prediction of a transition from the bright to the dark-exciton-dominated PL agrees well with the experiment and is yet further evidence of a phonon-bottleneck effect. Considering a fully thermalized Boltzmann distribution, there is no such transition, as shown in Figure 4c. The quantitative discrepancy between experiment and theory for the critical magnetic field value can be in part attributed to the higher effective exciton temperature predicted by the theory. The latter slightly overestimates the bright exciton population possibly due to small, temperature-dependent changes in the phonon dispersion or excitonic structure not accounted for in our model.

For a given perovskite, the difference between the bright-dark energy splitting Δ_{BD} and the optical phonon energy determines whether and at which temperature the bottleneck occurs. If there exists a phonon mode which couples to these excitons with an energy smaller than or resonant to Δ_{BD}, the bottleneck will not occur. In Figure 5, we show the effective exciton temperature as a function of the energy difference between the dominant longitudinal optical mode (E_{LO}) and the dark-bright exciton splitting Δ_{BD} for 100 K (green line) and 20 K (blue line). We find that for $(E_{LO} - \Delta_{BD}) \rightarrow 0$ the exciton temperature converges to the lattice temperature, as expected from a Boltzmann distribution. In contrast, as this energy difference increases, the effective exciton temperature grows larger demonstrating the existence of a phonon-bottleneck. We find the onset of this bottleneck to shift to lower Δ_{BD} the smaller the temperature is, as it becomes more difficult to overcome the energy offset with the thermal energy.

3. Discussion

We have explored exciton optics and dynamics in 2D perovskites, combining a sophisticated microscopic theory with cryogenic magneto-optical spectroscopy measurements. We determined the exciton fine-structure and the brightening of dark excitons in magneto-PL measurements. Contrary to previous studies focused on the relaxation of carriers and excitons from high energy bands to the minimum of bright exciton band[43,44] here we track the relaxation dynamics between the lowest energy dark and bright states having the dominant impact on the exerimentally accessible time-averaged emission. The exciton dynamics revealed from our simulations corroborate, both qualitatively and quantitatively, the experimentally observed time-averaged PL response, showing how a mismatch between the phonon energy and the splitting between bright and dark states gives rise to a pronounced phonon-bottleneck effect. This explains the observed unexpectedly strong emission of layered perovskites at low temperatures despite the dark ground state. The phonon-mode dictating the phonon-bottleneck originates is related to organic spacers.[45,46] Therefore, we predict that the chemical engineering of the organic spacer[47] can close or open the bottleneck. Overall, our joint theory-experiment study sheds new light on the population dynamics and optical response of layered perovskites,

crucial for optimizing the performance of perovskite-based devices.

4. Experimental Section

Exciton Fine-Structure: To model the optics and dynamics of excitons in layered perovskites, the Wannier equation[28] was first evaluated to derive the exciton binding energies and wavefunctions, taking into account screening from the lead-halide layer itself and from the organic spacer layers. More details could be found in the Supporting Information, including the form and parametrization[29,48] of this interaction. The study was restricted to 1s excitons, since the 1s-2s separation was very large (≈180 meV) compared to the exciton fine-structure including dark, bright and gray states. The 1s binding energy was determined to be 230 meV,[18,48] which was in good agreement with previous studies. While a monolayer perovskite is assumed, stacking additional layers had little effect on the band structure, owing to the separation introduced by the organic spacer layer.[49] The reduction in the excitonic binding energy from monolayer to bulk stems from the increased screening and was on the order of 10–20%,[35] which was much smaller than the monolayer-bulk comparison in other layered semiconductors, such as TMDs[50] exhibiting a reduction of up to 90%. The results were therefore valid for a larger number of perovskite layers, with increased screening reducing the exchange interaction, further enhancing the mismatch with the optical phonon energy and enhancing the bottleneck.

The exciton fine-structure was determined by both the spin-orbit coupling and the exchange interaction. In layered perovskites, the spin orbit coupling lead to a mixing of the orbital composition of the lowest conduction band,[11] which became a linear combination of *p*-orbitals. In contrast, there was no mixing of the valence band *s* orbitals. An expression for the exchange interaction in the excitonic basis was derived, taking into account the spin-orbit coupling in the conduction band. Details and the derivation can be found in the Supporting Information.

Exciton Optics: The absorption spectra of the perovskite monolayer could be calculated using the Elliot formula[28] where the absorption was described by a series of Lorentzian peaks centred at the exciton resonances which took into account both the radiative and non-radiative broadening. The absorption was calculated for σ-polarized light. The magnitude of the absorption signal was primarily determined by the optical matrix element. By taking into account the exchange interaction, the optical matrix elements and hence optical polarization of the excitonic states could be determined. The time-resolved photoluminescence could also be described using an Elliot formula, only now it was also proportional to the time-resolved occupation of the excitonic states, as detailed further in the Supporting Information.

Phonon-Driven Exciton Dynamics: A series of semiconductor Bloch equations was derived to capture the time evolution of the excitonic populations,[28,33] following optical excitation of the bright state X_+. The Heisenberg equation of motion, $i\hbar\partial_t N^n_{\mathbf{Q}} = \left\langle [N^n_{\mathbf{Q}}, \hat{H}_X] \right\rangle$ was employed to derive these equations. The second-order Born-Markov approximation[28] was applied to truncate the equations to the most important terms, taking into account the exciton-phonon interaction. Both the emission and absorption of optical and acoustic phonons was considered, allowing excitons to thermalize both in momentum and between excitonic bands. The optical phonons were particularly crucial in driving the exciton relaxation, owing to the strict momentum and energy conservation for the scattering processes. A detailed description was provided in the Supporting Information. Due to the strong spin-orbit coupling in these materials, the conduction band spin could be flipped in an exciton-phonon scattering event. For 2D perovskites, this process was necessary to enable phonon-scattering between the bright and dark/gray excitons.

Optical Spectroscopy: The photoluminescence was excited with a continuous wave laser emitting at 407 nm or second harmonic of pulsed fs-Ti: sapphire laser (450 nm, ∼150fs pulse duration). The sample was mounted inside a helium cryostat placed in a nitrogen-cooled pulsed magnet, providing a maximum field of 68 T with a pulse duration of 500 ms. The measurements were performed in the Voigt configuration, with the **c**-axis of the sample perpendicular to the magnetic field and parallel to the **k** vector of the exciting laser. Linear polarization was resolved in situ using a broadband polarizer.

Sample Fabrication: Glass substrates were ultrasonically cleaned sequentially using detergent solution, deionized water, acetone, and isopropanol. Subsequently, the substrates were dried in an oven T = 140 °C for ⩾10 min before treatment with ultraviolet ozone for 20 min. Immediately after cleaning, the substrates were placed in a nitrogen-filled glove box for film deposition. A stoichiometric precursor solution was used, prepared by dissolving PEA (Phenethylammonium iodide, 98.0% TCI) and PbI2 at a molar ratio of 2:1 in a mixed solvent of N,N'- dimethylformamide and dimethyl sulfoxide (4:1 volume ratio, 0.5 M concentration). To homogenize the solutions, they were stirred for at least 3 h at room temperature before deposition. A spin-coating process with antisolvent treatment was used to deposit the precursor solution onto the cleaned substrates. A rotation speed of 2000 rpm was used for the first 10 s of the spin-coating process. The speed was then accelerated to 8000 rpm for the remaining 30 s. Five seconds before the end of the spin-coating cycle, the antisolvent (chlorobenzene) was added to the substrate. The films were immediately annealed at 100 °C in a nitrogen atmosphere for 10 min.

Supporting Information

Supporting Information is available from the Wiley Online Library or from the author.

Acknowledgements

The authors acknowledged funding from the Deutsche Forschungsgemeinschaft (DFG) via SFB 1083 and the regular project 504846924. M.D. acknowledged support from the National Science Centre Poland within the SONATA grant (2021/43/D/ST3/01444). M.B. acknowledged support from the National Science Centre Poland within the OPUS LAP grant (2021/43/I/ST3/01357), and P.PL acknowledged support from the National Science Centre Poland within the MAESTRO grant (2020/38/A/ST3/00214). P.PE acknowledged support from the Polish National Agency for Academic Exchange within the Bekker program (BPN/BEK/2022/1/00120/U/00001).

Conflict of Interest

The authors declare no conflict of interest.

Data Availability Statement

The data that support the findings of this study are available from the corresponding author upon reasonable request.

Keywords

exciton dynamics, excitons, layered perovskite, phonons

Received: December 14, 2023
Revised: February 6, 2024
Published online:

[1] M. J. Schilcher, P. J. Robinson, D. J. Abramovitch, L. Z. Tan, A. M. Rappe, D. R. Reichman, D. A. Egger, *ACS Energy Lett.* **2021**, *6*, 2162.

[2] D. A. Egger, A. Bera, D. Cahen, G. Hodes, T. Kirchartz, L. Kronik, R. Lovrincic, A. M. Rappe, D. R. Reichman, O. Yaffe, *Adv. Mater.* **2018**, *30*, 1800691.
[3] H. Snaith, *Nat. Energy* **2019**, *4*, 1.
[4] Z.-K. Tan, R. S. Moghaddam, M. L. Lai, P. Docampo, R. Higler, F. Deschler, M. Price, A. Sadhanala, L. M. Pazos, D. Credgington, F. Hanusch, T. Bein, H. J. Snaith, R. H. Friend, *Nat. Nanotechnol.* **2014**, *9*, 687.
[5] P. Tamarat, L. Hou, J.-B. Trebbia, A. Swarnkar, L. Biadala, Y. Louyer, M. I. Bodnarchuk, M. V. Kovalenko, J. Even, B. Lounis, *Nat. Commun.* **2020**, *11*, 6001.
[6] R. Cai, I. Wadgaonkar, J. W. M. Lim, S. Dal Forno, D. Giovanni, M. Feng, S. Ye, M. Battiato, T. C. Sum, *Nat. Commun.* **2023**, *14*, 2472.
[7] Z. Yuan, C. Zhou, Y. Tian, Y. Shu, J. Messier, J. C. Wang, L. J. Van De Burgt, K. Kountouriotis, Y. Xin, E. Holt, K. Schanze, R. Clark, T. Siegrist, B. Ma, *Nat. Commun.* **2017**, *8*, 14051.
[8] H. Tsai, S. Shrestha, R. A. Vilá, W. Huang, C. Liu, C.-H. Hou, H.-H. Huang, X. Wen, M. Li, G. Wiederrecht, Y. Cui, M. Cotlet, X. Zhang, X. Ma, W. Nie, *Nat. Photonics* **2021**, *15*, 843.
[9] X. Gong, O. Voznyy, A. Jain, W. Liu, R. Sabatini, Z. Piontkowski, G. Walters, G. Bappi, S. Nokhrin, O. Bushuyev, M. Yuan, R. Comin, D. McCamant, S. O. Kelley, E. H. Sargent, *Nat. Mater.* **2018**, *17*, 550.
[10] P. Tamarat, M. I. Bodnarchuk, J.-B. Trebbia, R. Erni, M. V. Kovalenko, J. Even, B. Lounis, *Nat. Mater.* **2019**, *18*, 717.
[11] M. A. Becker, R. Vaxenburg, G. Nedelcu, P. C. Sercel, A. Shabaev, M. J. Mehl, J. G. Michopoulos, S. G. Lambrakos, N. Bernstein, J. L. Lyons, T. Stöferle, R. F. Mahrt, M. V. Kovalenko, D. J. Norris, G. Rainó, A. L. Efros, *Nature* **2018**, *553*, 189.
[12] M. Baranowski, P. Plochocka, *Adv. Energy Mater.* **2020**, *10*, 1903659.
[13] K. Tanaka, T. Takahashi, T. Kondo, K. Umeda, K. Ema, T. Umebayashi, K. Asai, K. Uchida, N. Miura, *Jpn. J. Appl. Phys.* **2005**, *44*, 5923.
[14] M. Fu, P. Tamarat, H. Huang, J. Even, A. L. Rogach, B. Lounis, *Nano Lett.* **2017**, *17*, 2895.
[15] M. Dyksik, H. Duim, D. K. Maude, M. Baranowski, M. A. Loi, P. Plochocka, *Sci. Adv.* **2021**, *7*, eabk0904.
[16] K. Posmyk, N. Zawadzka, M. Dyksik, A. Surrente, D. K. Maude, T. Kazimierczuk, A. Babiński, M. R. Molas, W. Paritmongkol, M. Mączka, W. A. Tisdale, P. Plochocka, M. Baranowski, *J. Phys. Chem. Lett.* **2022**, *13*, 4463.
[17] S. Kutkan, B. Dhanabalan, M.-L. Lin, P.-H. Tan, A. Schleusener, M. P. Arciniegas, R. Krahne, *Nanoscale* **2023**, *15*, 12880.
[18] D. B. Straus, S. Hurtado Parra, N. Iotov, J. Gebhardt, A. M. Rappe, J. E. Subotnik, J. M. Kikkawa, C. R. Kagan, *J. Am. Chem. Soc.* **2016**, *138*, 13798.
[19] J. M. Urban, G. Chehade, M. Dyksik, M. Menahem, A. Surrente, G. Trippé-Allard, D. K. Maude, D. Garrot, O. Yaffe, E. Deleporte, P. Plochocka, M. Baranowski, *J. Phys. Chem. Lett.* **2020**, *11*, 5830.
[20] F. Thouin, D. A. Valverde-Chávez, C. Quarti, D. Cortecchia, I. Bargigia, D. Beljonne, A. Petrozza, C. Silva, A. R. Srimath Kandada, *Nat. Mater.* **2019**, *18*, 349.
[21] M. Menahem, Z. Dai, S. Aharon, R. Sharma, M. Asher, Y. Diskin-Posner, R. Korobko, A. M. Rappe, O. Yaffe, *ACS Nano* **2021**, *15*, 10153.
[22] J. D. Ziegler, J. Zipfel, B. Meisinger, M. Menahem, X. Zhu, T. Taniguchi, K. Watanabe, O. Yaffe, D. A. Egger, A. Chernikov, *Nano Lett.* **2020**, *20*, 6674.
[23] P. C. Sercel, J. L. Lyons, D. Wickramaratne, R. Vaxenburg, N. Bernstein, A. L. Efros, *Nano Lett.* **2019**, *19*, 4068.
[24] A. Ghribi, R. Ben Aich, K. Boujdaria, T. Barisien, L. Legrand, M. Chamarro, C. Testelin, *Nanomaterials* **2021**, *11*, 3054.
[25] C. Quarti, G. Giorgi, C. Katan, J. Even, M. Palummo, *Adv. Opt. Mater.* **2023**, 2202801.
[26] K. Posmyk, M. Dyksik, A. Surrente, D. K. Maude, N. Zawadzka, A. Babiński, M. R. Molas, W. Paritmongkol, M. Mączka, W. A. Tisdale, P. Plochocka, M. Baranowski, *Adv. Opt. Mater.* **2023**, 2300877.
[27] T. T. H. Do, A. Granados del Aguila, D. Zhang, J. Xing, S. Liu, M. Prosnikov, W. Gao, K. Chang, P. C. Christianen, Q. Xiong, *Nano Lett.* **2020**, *20*, 5141.
[28] M. Kira, S. W. Koch, *Prog. Quantum Electron.* **2006**, *30*, 155.
[29] D. Feldstein, R. Perea-Causin, S. Wang, M. Dyksik, K. Watanabe, T. Taniguchi, P. Plochocka, E. Malic, *J. Phys. Chem. Lett.* **2020**, *11*, 9975.
[30] S. Koch, M. Kira, G. Khitrova, H. Gibbs, *Nat. Mater.* **2006**, *5*, 523.
[31] G. Biffi, Y. Cho, R. Krahne, T. C. Berkelbach, *J. Phys. Chem. C* **2023**, *127*, 1891.
[32] A. Surrente, M. Baranowski, P. Plochocka, *Appl. Phys. Lett.* **2021**, *118*, 17.
[33] S. Brem, M. Selig, G. Berghaeuser, E. Malic, *Sci. Rep.* **2018**, *8*, 8238.
[34] K. Wagner, J. Zipfel, R. Rosati, E. Wietek, J. D. Ziegler, S. Brem, R. Perea-Causín, T. Taniguchi, K. Watanabe, M. M. Glazov, E. Malic, A. Chernikov, *Phys. Rev. Lett.* **2021**, *127*, 076801.
[35] Y. Zhang, R. Wang, Y. Li, Z. Wang, S. Hu, X. Yan, Y. Zhai, C. Zhang, C. Sheng, *J. Phys. Chem. Lett.* **2018**, *10*, 13.
[36] A. Kiss, L. Szolnoki, F. Simon, *Sci. Rep.* **2016**, *6*, 22706.
[37] H.-H. Fang, J. Yang, S. Adjokatse, E. Tekelenburg, M. E. Kamminga, H. Duim, J. Ye, G. R. Blake, J. Even, M. A. Loi, *Adv. Funct. Mater.* **2020**, *30*, 1907979.
[38] M. I. Dar, G. Jacopin, S. Meloni, A. Mattoni, N. Arora, A. Boziki, S. M. Zakeeruddin, U. Rothlisberger, M. Grätzel, *Sci. Adv.* **2016**, *2*, 1601156.
[39] S. Kahmann, H. Duim, H.-H. Fang, M. Dyksik, S. Adjokatse, M. Rivera Medina, M. Pitaro, P. Plochocka, M. A. Loi, *Adv. Funct. Mater.* **2021**, *31*, 2103778.
[40] S. Hurtado Parra, D. B. Straus, B. T. Fichera, N. Iotov, C. R. Kagan, J. M. Kikkawa, *ACS Nano* **2022**, *16*, 21259.
[41] M. Fu, P. Tamarat, J.-B. Trebbia, M. I. Bodnarchuk, M. V. Kovalenko, J. Even, B. Lounis, *Nat. Commun.* **2018**, *9*, 3318.
[42] A. Shinde, P. K. Rajput, U. Makhija, R. Tanwar, P. Mandal, A. Nag, *Nano Lett.* **2023**, *23*, 6985.
[43] B. P. Carwithen, T. R. Hopper, Z. Ge, N. Mondal, T. Wang, R. Mazlumian, X. Zheng, F. Krieg, F. Montanarella, G. Nedelcu, M. Kroll, M. A. Siguan, J. M. Frost, K. Leo, Y. Vaynzof, M. I. Bodnarchuk, M. V. Kovalenko, A. A. Bakulin, *ACS Nano* **2023**, *17*, 6638.
[44] X. Jia, J. Jiang, Y. Zhang, J. Qiu, S. Wang, Z. Chen, N. Yuan, J. Ding, *Appl. Phys. Lett.* **2018**, *112*, 14.
[45] D. B. Straus, C. R. Kagan, *Annu. Rev. Phys. Chem.* **2022**, *73*, 403.
[46] M. Dyksik, D. Beret, M. Baranowski, H. Duim, S. Moyano, K. Posmyk, A. Mlayah, S. Adjokatse, D. K. Maude, M. A. Loi, P. Puech, P. Plochocka, *Adv. Sci.* **2023**, *11*, 2305182.
[47] Y. Boeije, W. T. Van Gompel, Y. Zhang, P. Ghosh, S. J. Zelewski, A. Maufort, B. Roose, Z. Y. Ooi, R. Chowdhury, I. Devroey, S. Lenaers, A. Tew, L. Dai, K. Dey, H. Salway, R. H. Friend, H. Sirringhaus, L. Lutsen, D. Vanderzande, A. Rao, S. D. Stranks, *J. Am. Chem. Soc.* **2023**, *145*, 21330.
[48] X. Hong, T. Ishihara, A. V. Nurmikko, *Phys. Rev. B* **1992**, *45*, 6961.
[49] Y.-Q. Zhao, Q.-R. Ma, B. Liu, Z.-L. Yu, J. Yang, M.-Q. Cai, *Nanoscale* **2018**, *10*, 8677.
[50] A. Chernikov, T. C. Berkelbach, H. M. Hill, A. Rigosi, Y. Li, B. Aslan, D. R. Reichman, M. S. Hybertsen, T. F. Heinz, *Phys. Rev. Lett.* **2014**, *113*, 076802.